P2.63 IWC AND ICE PRECIPITATION RETRIEVAL ALGORITHMS IN TERMS OF TEMPERATURE AND RADAR REFLECTIVITY USING OBSERVED ICE SPECTRA

Faisal S. Boudala*, George A. Isaac, and David Hudak

Cloud Physics and Severe Weather Research Section, Environment Canada, Toronto, Ontario, Canada

1. INTORODUCTION

Satellite observations and general circulation model (GCM) studies show that ice clouds have an important impact on earth's climate by influencing the radiation balance and hydrological cycle (e.g., *Ramanathan et al*. 1983; *Ramaswamy* and *Ramanathan* 1989). However, the value of ice water content (IWC) (e.g., *Stephens et al.* 2002) and precipitation simulated (*e.g., Ebert et al*. 2003) using the state of the art numerical models vary significantly. Occasional aircraft in-situ observations provide very useful information about the microphysical properties of clouds, but this data cannot validate climate models on a global scale. Radar technology is increasing being used for remotely retrieving cloud microphysical parameters. Since radar can be operated continuously, it can provide long term measurements of cloud properties. An experimental satellite, CloudSat, that was launched in 2006 (see *Stephens* et al. 2002), carries a 94 GHz radar. This radar should provide a global picture of cloud microphysical properties including IWC that can be used to constrain these models. However, radar measures the equivalent reflectivity factor (Z_e) of the cloud particles, but not their mass. The accuracy of the retrieved ice mass or ice precipitation rates based on radar reflectivity is highly dependent on the algorithms used. These algorithms are usually developed based on in-situ aircraft or ground measurements, or in combination with radar and in-situ measurements. In most cases, these retrieval algorithms include just one variable, Z_e. Generally, developing a parameterization based on both radar and aircraft in-situ data is not so trivial because of the difference in sampling volume and time lag associated with the two methods (e.g., *Hudak et al*. 2004). There are several IWC-Z_e power law relationships currently used to retrieve IWC, but a modeling study by *Sassen and Wang* (2002) shows that these power law relationships do not replicate the model calculations. *Brown et al.* (1995) showed that remotely retrieved IWC using a 94GHz radar can be accurate within a factor of 2 if Z_e alone is used, but this can be improved if the mean size of ice particles is included in the algorithm. Similarly *Liu and Illingworth* (2002) demonstrated that the inclusion of temperature can improve the accuracy of retrieved IWC.

There are several Z_e and ice mass flux (F_m) relationships (e.g., *Zawadzki et al.* 1993; *Sekhon and Serivastava* 1970; *Marshall and Palmer* 1948). However, they are not adequately validated against observations partly because of the scarcity of surface observation data, especially at high temporal resolution. Nonetheless, the available Z_e - F_m relationships do not explicitly include the effects of temperature. Recently, however, such a relationship has been developed (*Boudala et al.* 2006). In this paper, parameterization of IWC and ice precipitation retrieval algorithms that incorporate Z_e and temperature (T) will be presented based on the recent work *by Boudala et al.* (2006).

2. FIELD MEASUREMENTS

The data were collected during several projects using the National Research Council (NRC) Convair-580 aircraft. The FIRE Arctic Cloud Experiment (FIRE.ACE) project began in April 1998 and ended in July 1998, with the Convair-580 measurements being made in April (*Curry et al*. 2000). The First Canadian Freezing Drizzle Experiment (CFDE I) project was conducted in March 1995, and included numerous flights over Newfoundland and the Atlantic Ocean. The Third Canadian Freezing Drizzle (CFDE III) started in December 1997 and ended in February 1998. The first Alliance Icing Research Study (AIRS I) was conducted between 29 November 1999 and 19 February 2000 (*Isaac et al*. 2001b). The second AIRS (AIRS II) was conducted between November 2003 and February 2004 (*Isaac et al.* 2005). The Beaufort and Arctic Storms Experiment (BASE) field project was conducted in October 1994 over the Canadian Western Arctic (*Gultepe et al*. 2000). The data used in this paper is discussed in more details in *Boudala et al.* (2006).

The types of instrumentation used in these projects are described in *Isaac et al*. (2001a; 2001b; 2005) and *Boudala et al.* (2006). Nevzorov liquid water content (LWC) and total water content (TWC) probes (*Korolev*

* *Corresponding author address*: Faisal S. Boudala
Cloud Physics and Severe Weather Research Section, Environment Canada, Toronto, Ontario, Canada, M3H 5T4
E-mail: faisal.boudala@ec.gc.ca.

et al. 1998) which measure LWC and TWC respectively, and the PMS FSSP, 2D-C and 2D-P probes, which measure size, shape and concentration of hydrometers, were used. The temperature was measured with a Rosemount temperature probe.

During AIRS II, surface precipitation was measured using the Precipitation Occurrence Sensor System (POSS) that is described by *Sheppard* (1990). The POSS is X–band low power Doppler radar that measures the terminal velocity and size of cloud particles, as well as their reflectivity.

During the AIRS I field project, the McMaster University portable scanning X-band radar was deployed at ground level measuring cloud properties in coordination with aircraft measurements as described by *Hudak et al.* (2004). The radar scanned the cloud by a series of descending fixed-elevation stares of 90.0, 77.2, 61.5, 49.0, 39.1, 31.1, 24.8, 19.8, 15.0, 12.6 and 10.0 degrees. To match the radar data with the aircraft, the horizontal and vertical distance from the centre of the aircraft sample volume to the centre of the radar resolution cell was determined. In this work, only radar cells within a 1 km horizontal distance from center of aircraft sample volume have been used.

The identification of ice clouds follows the *Cober et al.* (2001) scheme. Based on this scheme, the stratiform ice clouds are characterized by FSSP concentration < 15 cm^{-3}, Rosemount icing detector < 2 mVs^{-1}, and Nevzorov LWC/TWC ratio <0.25. The temperature has been measured with a Rosemount temperature probe and the minimum temperature measured was near -40^{o}C.

3. IWC RADAR RETRIEVAL ALGORITHM

3.1 The Mass-Dimensional Relationship

Radar is used to measure reflectivity from an ensemble of particles. The retrieval of the mass of ice particles or precipitation rate depends on the type of parameterization that relates reflectivity (Z) to ice particle mass or ice precipitation rate. The derivation of IWC is sensitive to the assumed particle habit. Therefore, it is very crucial to select an appropriate particle habit that most likely represents the majority of the particle population. In-situ observations, however, indicate that most of the ice particles in the atmosphere are irregular in shape (*Korolev et al.* 2000), thus it is reasonable to represent ice particles by irregularly shaped or aggregate particles. There are, however, many types of aggregates that can be described as irregular in shape and characterized by differing mass-dimensional relationships (e.g., *Locatelli and Hobbs* 1974; *Cunningham* 1978; *Mitchell et al.* 1990). *Boudala et al.* (2002) found that the IWC derived using the Cunningham's coefficients, that relate the equivalent melted diameter to the measured cross-sectional area, showed a higher correlation with observations as compared to coefficients that relate the ice particle mass to its maximum or mean maximum diameter (*Mitchell et al.* 1990; *Locatelli and Hobbs* 1974).

Irregular ice particles can be represented by aggregates of plates and dendrites following *Boudala et al*. (2002; 2006) using the coefficients given in *Cunningham* (1978) as

$$D_e(A) = \begin{bmatrix} 0.39\,A^{0.31} & A \le 0.25\ mm^2 \\ 0.44A^{0.4} & \text{A}>0.25\ mm^2 \end{bmatrix}, \qquad (1)$$

where A is the cross-sectional area measured with optical array probes and D_e is the equivalent melted diameter of an ice particle. Using Eq. (1), the mass of a single ice particle can be given as

$$m(A) = \frac{a^3 \pi \rho A^{3b}}{6} \quad , \qquad (2)$$

where ρ is the density of liquid water. It is most convenient to use equivalent projected cross-sectional area diameter (D) of a circle such that $A = \pi D^2 / 4$ and transform Eqs. (1) and (2) into a form as

$$m(D) = \begin{bmatrix} 0.024D^{2.4} & 0.1\ mm<D \le 0.6mm \\ 0.0334D^{1.86} & D > 0.6mm \end{bmatrix}, \qquad (3)$$

where the mass is given in mg and D is given in mm. Note that the exponents in Eq. (3) are similar to coefficients derived based on in-situ observations in midlatitude ice clouds, recently reported by *Heymsfield* (2003)). This mass-dimensional relationship is give as

$$m(D) = 0.037 D^{2.25}, \qquad (4)$$

in the same units as Eq. (3). Figure 1a shows a comparison of IWC derived based on *Heymsfield* (2003) (Eq. 4) and *Cunningham* (1978) coefficients (Eq. 3) against the IWC measured with the Nevzorov probe. Each point in the figure represents an IWC derived using a 30s averaged ice particle spectra and the small ice particles are added following *Boudala et al.* (2002). The total data points shown in the figure are about 2036. There is no significant difference between these two schemes as long as D is the same in both cases, and both schemes agree quite well with the observation.

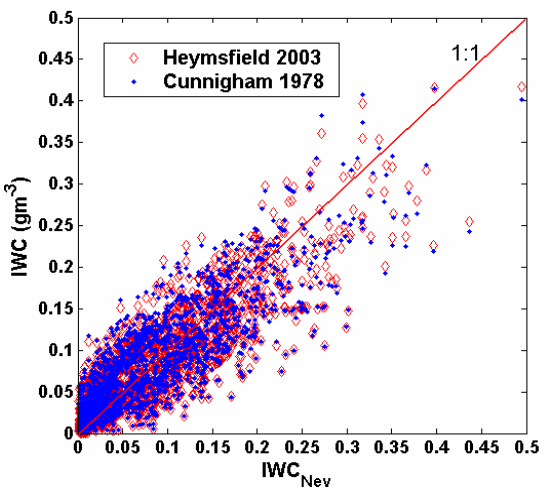

Figure 1a: IWCs measured with Nevzorov probe and derived based using 30s averaged ice spectra measured during CFDE (I and III), FIRE.ACE, and BASE using *Heymsfield* (2003) and *Cunningham* (1978) coefficients.

Using the relationships given in Eqs (3) and (4), it is straight forward to derive the mass and radar reflectivity of the measured ice particles, and this will be discussed in the following section. The contribution of small ice particles ($D \leq 100$ μm) are included following *Boudala et al.* (2002). However, the effect of the small particles on radar reflectivity factor is quite small.

3.2 *The Derivation of Radar Reflectivity Factor and IWC*

The distribution of ice particles $n(D)$ can be represented by a gamma distribution function in a form

$$n(D) = N_0 D^{\mu} \exp(-\lambda D), \tag{5}$$

where D is the equivalent cross-sectional area diameter of a circle, N_0 is the intercept parameter, μ and λ are the dispersion and slope parameters respectively. Assuming the mass-dimensional relation in a general form as

$$m(D) = \beta D^{\alpha} \quad , \tag{6a}$$

and using Eq. (5), the IWC can be derived following *Boudala et al.* (2006) as

$$\mathrm{IWC} = \frac{\beta N_0}{\lambda^{\alpha+\mu+1}} \Gamma(\alpha+\mu+1), \tag{6b}$$

where Γ is the gamma function. Similarly radar reflectivity can be calculated following *Heymsfield et al.* (2002a) using a Rayleigh scattering approximation as

$$Z = \left(\frac{6}{\rho\pi}\right)^2 \frac{N_0 \beta^2 \Gamma(2\alpha+\mu+1)}{\lambda^{2\alpha+\mu+1}} \tag{7}$$

where D_e is the equivalent melted diameter described earlier. Solving for λ in Eq. (6) and inserting into Eq. (7), IWC can be given in an alternate form following *Boudala et al.* (2006) as

$$\mathrm{IWC} = \kappa Z^{\gamma}, \tag{8}$$

where the exponent γ and κ are given as

$$\gamma = \frac{\alpha+\mu+1}{2\alpha+\mu+1}, \tag{9}$$

$$\kappa = \frac{\beta^{-\frac{(\mu+1)}{2\alpha+\mu+1}} N_0^{\frac{\alpha}{2\alpha+\mu+1}} \Gamma(\alpha+\mu+1)}{\left(\left(\frac{6}{\rho\pi}\right)^2 \Gamma(2\alpha+\mu+1)\right)^{\gamma}} \quad .$$

As shown in *Boudala et al.* (2006) if the dispersion (shape) parameter μ is set to zero an exponential distribution function, γ varies from 0.586 to 0.606 corresponding to α = 2.4 and 1.86 respectively, which is very close to 0.6. Actually, this can apply for most of the mass-dimensional relationships where α varies from 1.5 to 3 (*Locatelli and Hobbs* 1974; *Cunningham* 1978; *Mitchell et al.* 1990) resulting in an exponent change only from 0.625 to 0.571 respectively. Since the above expression for κ depends on $\beta^{-0.21}$ and $\beta^{-0.17}$ depending on which α is used, it is relatively insensitive to the particle habit. However, the dispersion parameter μ could be important in modifying the exponents in the expression given in Eq. (7). Based on midlatitude data, *Heymsfield et al.* (2002b) showed that the dispersion parameter generally increases with decreasing temperature. For a given m-D relationship (see Eq. 3), it is possible to derive μ using the equation provided by *Mitchell* (1991) as

$$\mu = \frac{(\alpha+0.67)\bar{D} - D_m}{D_m - \bar{D}} \tag{10}$$

where D_m is the median mass diameter and $\bar{D}$ is the mean diameter that can be derived as

$$\bar{D} = \frac{\sum_{D_{\min}}^{D_{\max}} DN(D)}{\sum_{D_{\min}}^{D_{\max}} N(D)} . \qquad (11a)$$

Both $\bar{D}$ and D_m can be calculated using ice particle spectra measured with optical array probes.

Figure 1b shows $\bar{D}$ (panel a) and μ (panel b) plotted against temperature as derived based on 2D-C and 2D-P probe measurement data shown in Fig. 1a.

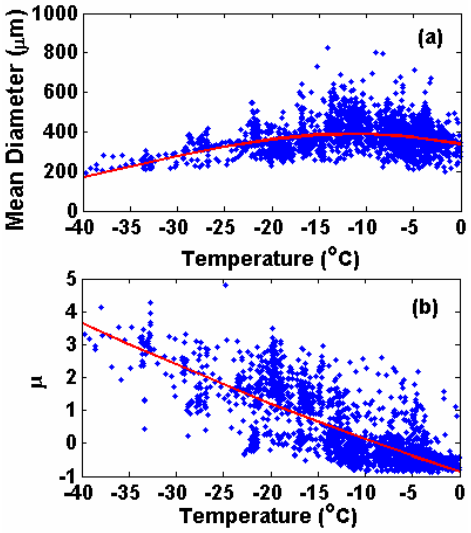

Figure 1b: The mean diameter (a) and dispersion coefficient (b) derived using Eq. 4 and Eq. 10 are plotted against temperature.

On average, the mean diameter of ice particles increases with increasing temperature as would be expected showing a slight maximum near -12 °C where a maximum in supersaturation with respect to ice is expected. The mean square fit line to the data is given as

$$\bar{D} = 343.0582 \exp(-0.001T^2 - 0.0232T) \qquad (11b)$$

In contrary to the mean diameter, the dispersion parameter increases with decreasing temperature in agreement with the finding reported by *Heymsfield et al.* (2002). The mean square fit line in panel b is given as

$$\mu = 5.1456\text{E-}4T^2 - 0.0925T - 0.8446 \qquad (11c)$$

Knowing μ and $\bar{D}$, it is possible to derive the other coefficients mentioned in Eq. 5 using the relationships given *Mitchell* (1991).

3.3 Radar Reflectivity Based On Aircraft Measurements

It is convenient to write Eq. (7) in a form

$$Z = \left(\frac{6}{\rho\pi}\right)^2 \sum_{D_{\min}}^{D_{\max}} N(D) m^2 , \qquad (12)$$

to derive radar reflectivity using aircraft data, where ρ is the density of water and m is given in Eq.(3) or Eq. (4). Figure 2 is taken from *Boudala et al.* (2006) and shows derived IWC plotted against derived Z based on Eq. (3) using the 30s averaged ice particle size spectra measured with the PMS 2D-C and 2D-P during several field projects. For a given IWC, Z generally increases with increasing temperature. This is consistent with the fact that the mean size of ice particles increases with increasing temperature, which also increases Z. The power law relationships for each temperature interval are also given in the figure. The power law coefficients are increasing with decreasing temperature. For example, γ varies from 0.4 to 0.7 as opposed to just 0.6 as predicted using an exponential function (Eqs. 8 and 9).

Figure 3 shows γ calculated using the same data set, but by setting $\alpha = 2.4$ for the entire spectrum in Eq. (9) since this assumption gave approximately the same IWC as compared to the IWC derived using Eq. (3).

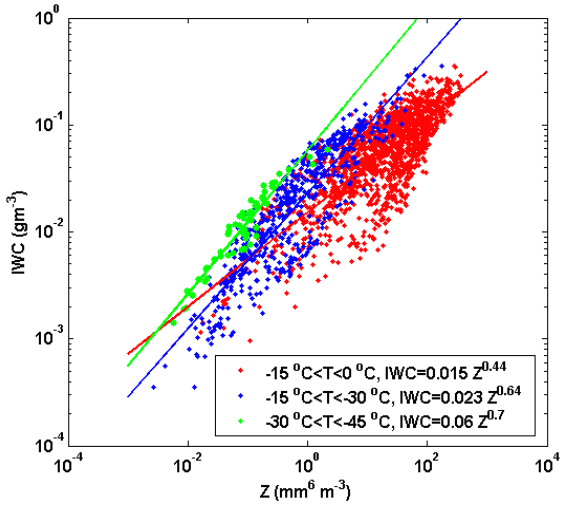

Figure 2: IWC and Z derived using 30s averaged spectra measured during the CFDE (I and III), FIRE.ACE and BASE projects are plotted for various temperature intervals.

As indicated in the figure, γ increases with decreasing temperature which is consistent with Fig. 2. However, it

is worth mentioning that there is a great deal of scatter in γ, as indicated in Fig. 3, which makes it difficult for the development of an accurate parameterization of an IWC retrieval algorithm using radar reflectivity. However, to a first approximation one can use a linear fit in order to get the approximate value of γ for a given temperature.

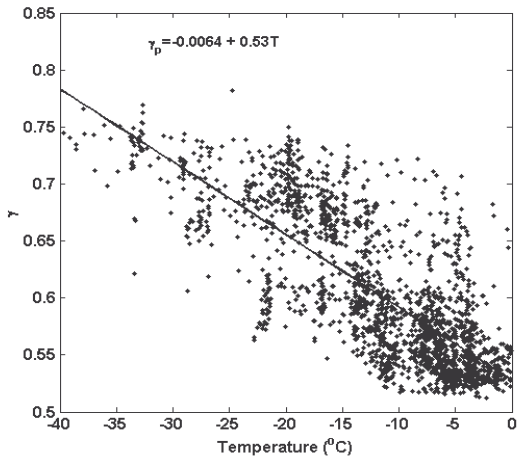

Figure 3: The exponent γ given in Eq. (8) is plotted as a function of temperature.

Inspecting Eq. (9), κ depends on the intercept parameter N_0 and μ. Previous studies by *Heymsfield et al.* (2002b) and *Ryan* (2000) showed that N_0 depends on temperature. In order to assess the temperature dependence of κ, the ratio IWC/Z^{γ} is plotted against temperature in Fig. 4 by setting $\gamma = \gamma(\mathrm{T})$ as given in Fig. 3. κ increases with decreasing temperature and this is also consistent with Fig. 2.

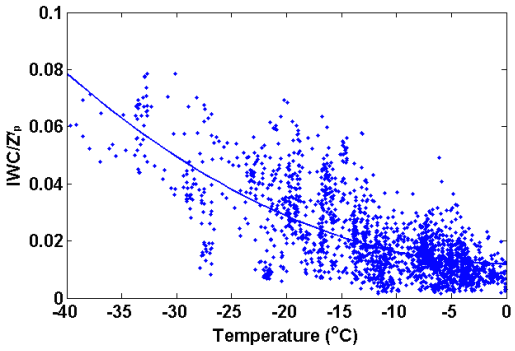

Figure 4: The ratios $\mathrm{IWC}/Z^{\gamma(\mathrm{T})}$ derived from 30s averaged ice spectra measured during the CFDE (I and III) , FIRE.ACE and BASE projects are plotted against temperature.

Inspecting Fig. 4, the fitted lines follow a polynomial function of temperature. Therefore, a parameterization is proposed as:

$$\mathrm{IWC} = (6.783x10^{-5}\mathrm{T}^2 + 0.0262)Z^{(-0.0064T+0.4)}, \quad (13a)$$

where T is the temperature in ^{o}C and Z is given as mm^6 m^{-3}, and IWC is given in gm^{-3}.

4. TESTING THE PARAMETERIZATION

The IWC retrieval algorithms currently employed in radar remote sensing application are mainly based on mm wave radar reflectivity measurements, thus they are not directly applicable for Z_e determined using the Raleigh scattering approximation. Some of these IWC-Z_e relationships are summarized in *Sassen and Wang* (2002). Generally, Z determined based on a Rayleigh approximation is corrected using Mie scattering theory using a formula as

$$Z_{\mathrm{Mie}} = \left(\frac{6}{\rho\pi}\right)^2 \sum_{D_{\min}}^{D_{\max}} N(D)m^2 f(D), \quad (13b)$$

where $f(D) = \sigma_{Mie}/\sigma_{Ray}$, and the coefficients σ_{Mie} and σ_{Mie} are backscatter cross-sections calculated based on a Rayleigh and Mie scattering model for a given radar frequency respectively. Figure 5a shows the calculated $f(D)$ for a 94 GHz frequency radar assuming spherical ice and liquid particles at two different temperatures and the corresponding dielectric constants are also given.

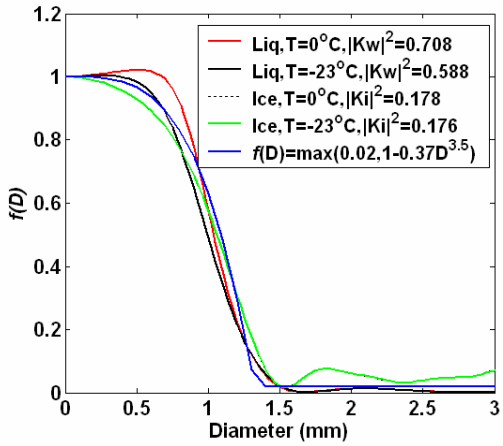

Figure 5a: The ratio of calculated back scattered cross-section $f(D) = \sigma_{Mie}/\sigma_{Ray}$ using Mie and Rayleigh models at 94 GHz are plotted against diameter. K_i and K_i are the dielectric constants for ice spheres (*Mätzler* (1998) and liquid drops (*Liebe et al.* 1991).

The Mie backscattering calculation was based on *Bohren and Huffman* (1983). The dielectric constants are based on *Mätzler* (1998) for ice and *Liebe et al.*

(1991) for liquid water. At 94 GHz, the Rayleigh scattering approximation is only valid for D smaller than about 0.6 mm. However, for D greater than 0.6 mm, the Rayleigh scattering approximation significantly overestimates Z. It should be noted that at this radar frequency, the temperature dependence of $f(D)$ is relatively weak, particularly, for ice particles. Therefore, it is possible to express $f(D)$ with a simple function as shown in the figure. Using this expression for $f(D)$ and Eq. 13b, *Boudala et al.* (2006) derived a relationship between Z_{Mie} (Z_{94}) and Z based on the measured ice particle spectra as

$$Z=1.0681 Z_{94}^{1.0612}. \qquad (13c)$$

The correction factor for low Z values ($Z < 2$ mm^6 m^{-3}) appears to be negligible based on this analysis. At Z = 10 mm^6 m^{-3}, Z_{94} is about 18% lower than Z. This power law relationship is found between Z_{94} and Z can be applied to correct for Z when 94 GHz measurements are being used.

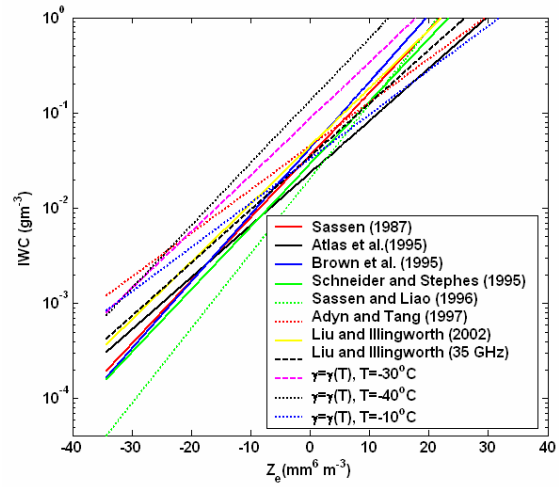

Figure 5b: Various IWC-Z relationships and the parameterization developed in this work.

Figure 5b shows comparisons of the IWC-Z_e relationships taken from *Sassen and Wang* (2002). Since these relationships only involve Z_e, it is rather difficult to plot them together with the new parameterizations. However, the parameterizations developed above for temperatures -10 °C, -30 °C, and -40 °C are shown for comparison. Furthermore, Z has to be converted to equivalent radar reflectivity factor (Z_e) following the convention given in Appendix A (*Boudala et al.* 2006). At relatively high values of Z, most of the IWC - Z relationships lie within the IWC values calculated using the new parameterization. At low values of Z_e, however, the new parameterization gives higher IWC as compared to most of the conventional relationships. Therefore, the discrepancy among these relationships may not be explained based on the temperature alone. The new parameterization for temperatures lower than -40 °C were not shown for consistency, since we don't have in-situ observations for lower temperatures for validation.

Figure 6 shows the IWC measured with a Nevzorov probe during the First Alliance Icing Research Study (AIRS I) plotted against the retrieved IWCs based on the IWC-Z_e relationships using the 10 GHz McMaster radar data mentioned in Section 2. Also shown are the IWC estimates from the radar data using the parameterization developed in this paper. The results using the conventional IWC-Z_e relationships overestimate the ice mass at higher Z_e values and underestimate it at lower Z_e values, while the parameterization from this paper appear to fit better the one-to-one line. There is considerable scatter for all methods suggesting that the parameterization based on Z_e alone appears to be inadequate. However, it should be noted that the accuracy of the direct measurements have some errors, thus more studies are required for further validation of the new parameterization.

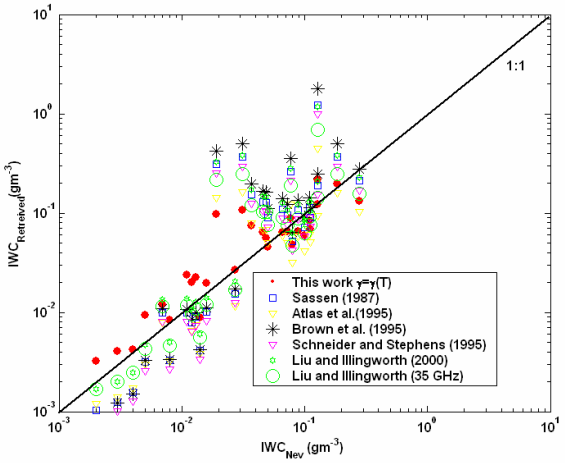

Figure 6: The IWCs retrieved based on observed temperature and Z measured with radar are plotted against the IWC measured with the Nevzorov probe during the AIRS I project.

5. PRECIPITATION

Using the gamma distribution function discussed earlier and an empirical terminal velocity versus diameter relationship, *Boudala et al.* (2006) shown that the downward ice mass flux can be given as

$$F_m = \left(\frac{\rho_o}{\rho_a}\right)^{1/2} \frac{a'\beta N_0 \Gamma(\alpha+\mu+b'+1)}{\lambda^{\alpha+\mu+b'+1}} \qquad (14)$$

where a' and b' are coefficients associated with terminal velocity ($v = a' D^{b'} (\rho_o / \rho_a)^{1/2}$ see Eq. 18), and the other symbols mean the same as in section 3.1. After substituting the slope parameter from Eq. (6) in into Eq. (14), the downward ice mass flux can be given as

$$F_m = \Omega Z^{\omega}, \tag{15}$$

where the parameters Ω and ω are given as

$$\Omega = \frac{a' \beta^{\frac{-(\mu+2b'+1)}{2\alpha+\mu+1}} N_0^{\frac{(b'+\alpha)}{2\alpha+\mu+1}} \Gamma(\alpha+\mu+b'+1)}{\left[\left(\frac{6}{\rho\pi}\right)^2 \Gamma(2\alpha+\mu+1)\right]^{\frac{\alpha+\mu+b'+1}{2\alpha+\mu+1}}} \tag{16}$$

and

$$\omega = \frac{\alpha+\mu+b'+1}{2\alpha+\mu+1} \tag{17}$$

If the shape parameter is set to zero, and b'=0.27 assuming aggregates of densely rimed radiating assemblages of dendrites (*Locatelli and Hobbs* 1974) (see Eq. 18 below) and setting α=2.25 (*Heymsfield* 2003), Ω is related to the mass and intercept parameter as $\beta^{-0.28}$ and $N_0^{0.46}$ indicating that there is stronger dependence on N_0 than the assumed particle habit. However, since Ω is directly proportional to a', there is a stronger dependence on terminal velocity than the mass. The exponent ω in this case is 0.64 that is very similar to the so called Marshall-Palmer $Z - F_m$ relationship (*Marshall and Palmer* 1948) based on measurements of raindrop size distributions, which uses 0.63. However, using the same arguments as before, Eqs. (16) and (17) should depend on temperature. Furthermore, based on surface measurements, the dependence of stratiform precipitation amount on temperature has been shown (*Isaac and Stuart* 1996; *Isaac and Stuart* 1992).

Figure 7 shows the derived ice mass flux plotted against reflectivity for a given temperature interval. The downward ice mass flux was calculated using the same data set discussed above assuming a terminal velocity v corresponding to aggregates of densely rimed radiating assemblages of dendrites (*Locatelli and Hobbs* 1974) given as

$$v = 0.79 D^{0.27} \left(\rho_o / \rho\right)^{1/2}, \tag{18}$$

where D is in mm and v is in m s^{-1}, $\rho_0 = 1$ is the reference density, ρ_a is the air density. This result also demonstrates the dependence of mass flux on temperature. For a given F_m, increasing temperature increases the reflectivity as a result of the increase in particle size with temperature, which is similar to Fig. 2. The change of ω with temperature in Eq. (17), appears to be mainly due to a change in the dispersion of the ice particle distribution as demonstrated in Fig. 8, which shows ω plotted as a function of temperature. As in the case of Fig. 3, the data shows significant scatter, but the variation in ω with temperature has similar trends as the $Z - F_m$ relations shown in Fig. 7.

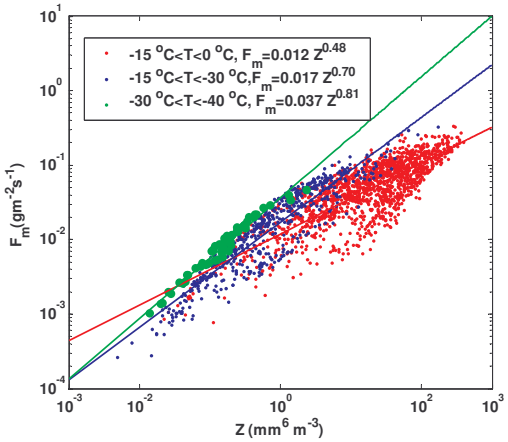

Figure 7: Downward ice flux calculated based on the terminal velocity given in Eq. (18) and 30s averaged ice spectra measured during the CFDE (I and III), FIRE.ACE, and BASE projects.

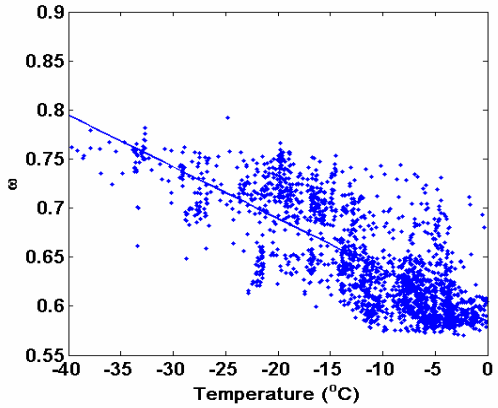

Figure 8: The exponent ω derived based on Eq. (16) using 30s averaged spectra measured during CFDE (I and III), FIRE.ACE and BASE plotted against temperature.

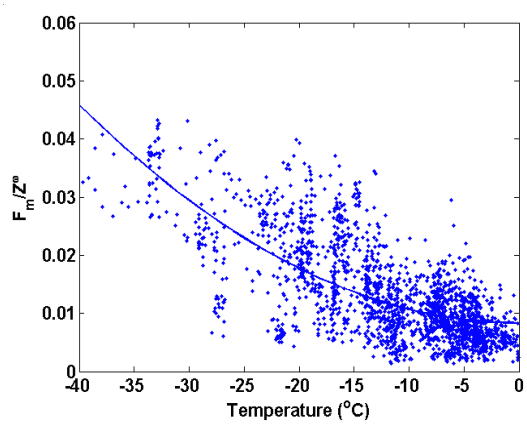

Figure 9: The ratios $F_m/Z^{\omega(T)}$ derived from 30s averaged ice spectra measured during CFDE (I and III), FIRE.ACE, and BASE plotted against temperature.

In order to find the dependence of Ω on temperature, the ratios of $F_m/Z^{\omega(T)}$ were plotted against temperature in Fig. 9. There is clearly a nonlinear dependence on temperature. Therefore, we propose similar functional relationships as Eq. (13) and the parameterized precipitation rate (F_m) is given as

$$F_m = (6.85x10^{-5}T^2 + 0.0464)Z^{-0.006T+0.48}, \qquad (19)$$

where the temperature T is given ^oC , Z is $mm^6\ m^{-3}$, and F_m is given in $mm\ h^{-1}$.

In the US operational forecast, the snow fall rate is normally estimated using a formula $F_m=kZ^{0.5}$ where k varies anywhere form 0.0577 to 0.0877 depending on the intensity (*Super and Holyroyd* 1997). When compared at the same units, it is interesting to note in Fig. 7 that k varies from 0.04 to 0.1 depending on temperature, which is similar to the k range mentioned above.

The current radar remote sensing algorithm used in most of the Canadian radar community is based on *Sekhon and Srivastava* (1970) and this is given as

$$F_{ss} = 0.034Z^{0.45}, \qquad (20)$$

where Z is $mm^6\ m^{-3}$, and F_{ss} is given mmh^{-1} . It is also interesting to note that this expression is similar to the power law relationship given in Fig. 7 for temperatures between 0 ^oC and -15 ^oC when compared at the same units, which would be $F_m = 0.043Z^{0.48}$ (see Fig. 7). For other temperature intervals, however, there are significant differences. The parameterization developed by Sekhon and Srivastava is based on a assumed exponential ice particle size distribution. In this exponential size distribution, the slope parameter is related to ice precipitation rate. The expression given in Eq. (20) underestimates the precipitation rate even for warm temperatures as compared to Eq. (19) or Fig. 7. This discrepancy between these two parameterizations, could be partly explained due to the difference in parameterization of the slope and intercept parameters. Based on measured spectra, we have shown for a given precipitation rate, the reflectivity increases with increasing temperature. Therefore, the slope of the F_m - Z power low curve increases with decreasing temperature, thus a single power law curve such as given in Eq. (20) is not appropriate for all temperatures. It should be mentioned that when Z is measured with a high frequency radar, such as 94 GHz, similar corrections like Eq. 13c have to be applied in Eq. 19 before the parameterizations are applied.

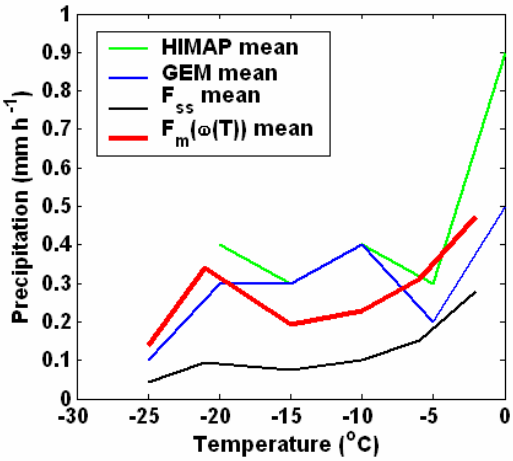

Figure 10: The mean precipitation rates retrieved using POSS reflectivity measurements at the surface level based on a new parameterization developed in this work (Eq.19) and the algorithm developed by *Sekhon and Srivastava* (1970) (Eq. 20) are compared to model predictions during the AIRS II project.

Figure 10 shows the averaged precipitation rates based on remote sensing using the parameterization developed in this work, *Sekhon and Srivastava* (1970), and predicted using models at the surface level. The surface precipitation calculations are made using reflectivity measurements made by Precipitation Occurrence Sensor System (POSS). The model predictions were made using the Canadian regional model at 24 km resolution (GEM) and at 10 km resolution (HIMAP) during the Second Alliance Icing Research Study (AIRS II) project. The precipitation rates are averaged in 5 ^oC temperature interval. On average, the mass flux (precipitation rate) increases with increasing temperature. The precipitation rate retrieved using the *Sekhon and Srivastava* (1970) scheme underestimates the precipitation rate as compared to the models and the new parameterization. However, the mean precipitation rates derived based on

the new parameterization are reasonably close to the model predicted values.

6. SUMMARY AND CONCLUSIONS

The accuracy of the numerical model prediction of climate and weather depends on their treatment of ice phase clouds. The model simulations of IWC and ice removal rate using the current numerical weather prediction and climate model differ significantly from one to the other. One way to validate and constrain these models is to measure these quantities on a global scale. However, this approach is not achievable by conventional means such as occasional aircraft measurements. Radar technology offers a great hope for continued remote sensing of cloud microphysical properties over vast geographical regions. CloudSat (*Stephens et al*. 2002), which was launched in 2006 carrying a 94 GHz radar, is one example for providing such measurements. However, the radar remote sensing algorithm currently used to retrieve IWC and precipitation are mainly based on the equivalent reflectivity factor (Z_e) alone. In this paper, a parameterization of radar retrieval algorithms of IWC and ice precipitation rate as a function of temperature and Z have been discussed based on results reported in *Boudala et al.* (2006).

These parameterizations were developed using in-situ aircraft measurements conducted in stratiform clouds over large areas of midlatitude and Arctic regions. The parameterizations are well correlated with IWC and precipitation rate derived directly from measured ice spectra obtained during the CFDE (I and III), BASE, and FIRE.ACE field projects with correlation coefficients (r) near 0.8 (see *Boudala et al*. 2006).

The parameterizations are also tested based on X-band and Doppler radar equivalent reflectivity, temperature, and IWC measurements during the First and Second Alliance Icing Study projects (AIRS I and II). The retrieved IWCs using the X-band radar agreed reasonably well with IWCs directly measured with Nevzorov probe during AIRS I project. This study shows that the conventional IWC- Z_e relationships currently used in remote sensing applications don't seem to agree with the Nevzorov probe measurements.

The new and standard precipitation retrieval algorithm currently in use in Canada, were also tested using the Doppler radar known as the Precipitation Occurrence Sensor System (POSS) using the AIRS II data. It was shown that the precipitation retrieval algorithm currently in use in Canada underestimates the ice precipitation rate as compared to the regional weather prediction models. Therefore, this study suggests that the climatologically data collected thus far and the current public ice precipitation forecast in Canada may have been significantly underestimated. However, since there are some uncertainties in the direct measurements of IWC and no reliable direct measurements of precipitation rate are available, further studies are required to validate these parameterizations.

7. ACKNOWLEDGEMENTS

This work was funded by the National Search and Rescue Secretariat, Transport Canada, the Panel on Energy Research and Development, the Canadian Climate Action Fund, the Natural Sciences and Engineering Research Council, as well as from U.S. sources including the Boeing Commercial Airplane Group, the National Aeronautics and Space Administration, and the Federal Aviation Administration, The data were collected using the Canadian National Research Council Convair-580 and the authors are grateful to their NRC colleagues for their assistance. Faisal Boudala also received funds from the National Science and Engineering Research Council (NSERC) and the Canadian Foundation for Climate and Atmospheric Sciences (CFCAS).The authors also thank Brian Sheppard for processing the POSS data, Janti Reid for providing the surface precipitation data collected during the AIRS II project, and Peter Rodriguez for providing the AIRS I radar data..

8. REFERENCES

Arnott, W. P., D. Mitchell, C. Schmitt, D. Kingsmill, D. Ivanova, and M. R. Poellot, 2000: Analysis of FSSP performance for measurement of small crystal spectra in cirrus. *Proceedings 13th Intl. Conf. on Clouds and Precipitation*, Reno Nevada, 14-18 August 2000, 191-193.

Atlas, D., S. Y. Matrosov, A. J. Heymsfield, M.-D. Chou, and D. B. Wolf , 1995: Radar and radiation properties of ice clouds. *J. Appl. Meteor.,* ***34***, 2329–2345.

Aydin, K., and C. Tang ,1997: Relationships between IWC and polarimetric radar measurements at 94 and 220 GHz for hexagonal columns and plates. *J. Atmos. Oceanic Technol.,* ***14*****,** 1055–1063.

Baumgardner, D. (1983), Analysis and comparison of five water droplet measuring devices. *J. Climate Appl. Meteor*., **22**, 891-910.

Baumgardner, D., and M. Spowart, 1990: Evaluation of Forward Scattering Spectrometer Probe. Part III: Time response and laser inhomogeneity limitations. *J. Atmos. Oceanic Technol*., **7**, 666-672.

Bohren C.F. and D.R. Huffman, 1983: Absorption and Scattering of Light by Small Particles, John

Wiley, New York, NY.

Boudala, F. S., A. G. Isaac, and D. Hudak, 2006: Ice water content and precipitation rate as a function of equivalent radar reflectivity and temperature based on in-situ observations. *J. Geophysical Research*. In press.

Boudala, F. S., A. G. Isaac, Q. Fu, and S. G. Cober , 2002, Parameterization of effective particle sizes for high latitude clouds. *Int. J. Climatology*, **22**, 1267-1284.

Brown, P. R., A. J. Illingworth, A. J. Heymsfield, G. M. McFarquhar, K. A. Browning, and M. Gosset, 1995: The role of space borne millimeter-wave radar in the global monitoring of ice cloud. *J. Appl. Meteor.,* **34,** 2346–2366

Cober, S. G., G. A. Isaac, A.V. Korolev, and J.W. Strapp, 2001:Assessing cloud-phase conditions *J. Appl. Meteor*., **40***,* 1967-1983**.**

Curry, J. A., P. V. Hobbs, M. D. King, D. A. Randall, P. Minnis, G. A. Isaac, J. O. Pinto, T.Uttal, A. Bucholtz, D. G. Cripe, H. Gerber, C. W. Fairall, T. J. Garrett, J. Hudson, J. M. Intrieri, A. Jakob, T. Jensen, P. Lawson, D. L. Marcotte, L.Nguyen, P. Pilewskie, A. Rangno, A. B. Rogers, K. B. Strawbridge, F. P. J. Valero, A. G. Williams, and D. Wylie, 2000: FIRE Arctic Clouds Experiment. *Bull. Am. Meteorol. Soc.*, ***81***, 5-29.

Cunningham M. R., 1978: Analysis of particle spectral data from optical array (PMS) 1D and 2D sensors. American Meteorological Society, Fourth Symposium . Meteorol. Obs. Instrument. Denver, USA, April 10-14, 1978, 345-350.

Ebert, E. E., U. Damrath, W. Wergen, and M. E. Baldwin, 2003:The wagne assessment of short term quantitative precipitation forecasts. *Bull. Amer. Meteor. Soc., **84*,** 481-492

Field, P. R., R. Wood, and A. R. P. Brown ,2003: Ice particle interval rimes measured with FSSP. *J. Atmos. Oceanic Technol*., ***20***, 249-261.

Gardiner, B. A. and J. Hallett, 1985: Degradation of in cloud Forward Scattering Spectrometer Probe measurements in presence of ice particles. *J. Atmos. Oceanic Technol*., **13,** 1152-1165.

Brenguier, J. L. ,1989: Coincidence and dead time corrections for particle counters. Part II: High concentration measurements with FSSP. *J. Atmos. Oceanic Technol*., **6**, 585-598.

Gultepe, I., G. A. Isaac, D. Hudak, R. Nissen, and J. W. Strapp, 2000: Dynamical and microphysical characteristics of Arctic clouds during BASE. *J. Climate*, **13**, 1225- 1254.

Heymsfield, A. J. , 2003: Properties of tropical and midlatitude ice clouds particle ensembles. Part I: Median mass diameter and terminal velocities. *J. Atmos. Sci*., ***60***, 2573-2591.

Heymsfield, A J, M. Kajikawa, C. Twohy, and M. R. Poellot (2002a), A general approach for deriving the properties of cirrus and stratiform ice cloud particles. *J. Atmos. Sci., **59*,** 3-29.

Heymsfield, A. J., A. Bansemer, P. R. Field, S. L. Durden, J. Stith, J. E. Dye, and W. Hall (2002b), Observations and parameterizations of particle size distributions in deep tropical cirrus and stratiform clouds: Results from in situ observations in TRMM field campaigns. *J. Atmos. Sci., **59*,** 3457–3491.

Hudak, D.R., P. Rodrigez, M. Wolde, B. Currie, S. Cober, I. Zawadzki., and G. Isaac ,2004: Evaluation of ground based data and in-situ aircraft data comparison in winter storms. 14th *Int. Conf. on Clouds and Precipitation (ICCP)*, Bologna, Italy, 796-799.

Isaac, G.A., A.V. Korolev, J.W. Strapp, S.G. Cober, F.S. Boudala, D. Marcotte and V.L. Reich, 2006: Assessing the collection efficiency of natural cloud particles impacting the Nevzorov total water content probe. AIAA 44th Aerospace Sciences Meeting and Exhibit, Reno, Nevada. 9-12 January 2006. AIAA-2006-1221.

Isaac, G. A., J. K. Ayers, M. Bailey, L. Bissonnette, B.C. Bernstein, S. G. Cober, N. Driedger, W.F. J. Evans, F. Fabry, A.Glazer, I. Gultepe, J. Hallet, D. Hudak, A.V. Korolev, D. Marcotte, P. Minnis, J. Murray, L. Nyguyen, T. P. Ratvasky, A. Reehorst, J. Reid, P. Rodriguez, T. Schneider, B. E. Sheppard, J. W. Strapp, and M. Wolde, 2005: First results from the Alliance Icing Research Study (AIRS). AIAA 43th Aerospace Sciences Meeting and Exhibit, Reno, Nevada, 11-13 January 2005.

Isaac, G. A., S. G. Cober, J. W. Strapp, A.V. Korolev, A. Tremblay, and D. L. Marcotte, 2001a: Recent Canadian research on aircraft in-flight icing. *Canadian Aeronautics and Space Journal*, 47-3, 213-221.

Isaac, G. A., S.G. Cober, J. W. Strapp, and D. Hudak, 2001b: Preliminary Results from Alliance Icing Research Study (AIRS). AIAA 39th Aerospace Sciences Meeting and Exhibit, Reno, Nevada. 8-12 January 2001

Isaac, G. A, and R. A. Stuart, 1996: The relationship between cloud type and amount, precipitation, and surface temperature in the Mackenzie River valley-Beaufort area. *J. Climate* , **9**, 1921-1941.

Isaac, G. A, and R. A. Stuart, 1992: Temperature precipitation relationships for Canadian stations. *J. Climate* , *5*, 822-830.

Knollenberg, R.G., 1970: The optical array: An alternative to scattering or extinction for airborne particle size determination. *J. Appl. Meteor*., *9*, 86-103.

Korolev, A. V., W. J. Strapp, and G. A. Isaac, 1998: Evaluation of accuracy of PMS optical array probe. *J. Atmos. Oceanic Technol*., ***15***, 708-720.

Korolev, A., G.A. Isaac, and J. Hallett, 2000: Ice particle habits in stratiform clouds. *Quart. J. Roy. Meteor. Soc.*, *126*, 2873-2902.Lau, K. -M., Y. S. Sud, and J. H. Kim, 1995: Intercomparison of hydrologic processes in global climate models. NASA Tech. Memo. 104617, 161 pp.

Liebe H.J., G.A. Hufford and T. Manabe ,1991: A model for the complex permittivity of water at frequencies below 1 THz, Internat. J. Infrared and mm Waves, Vol. 12, pp. 659-675..

Liu, C., and A. J. Illingworth, 2000: Toward more accurate retrievals of ice water content from radar measurements of clouds. *J. Appl. Meteor.,* ***39*****,** 1130–1146.

Locatelli, J. D. and P. V. Hobbs ,1974: Fall speeds and masses of solid precipitation particles. J. Geophys. Res., **79**, 2185-2197

Marshall, J. S., and W. McK. Palmer, 1948: The distribution of rain drops with. J. Meteor., **5**, 165-166

Mätzler C , 1998: Microwave properties of ice and snow, in B. Schmitt et al. (eds.), Solar System Ices, Astrophys. and Space Sci. Library, Vol. 227, Kluwer Academic Publishers, Dordrecht, pp. 241-257

Mitchell, D. L. , 1991: Evolution of snow size spectra in cyclonic stroms. Part II: Deviations from exponential forms. J. *Atmos. Sci*., **48**, 1885-1899.

Ramanathan, V., J. Pitcher, R. C. Malone and M. L. Blackmon ,1983: The response of a spectral general circulation to refinements in radiative processes. *J. Atmos. Sci*., **40**, 605 – 630.

Ramaswamy, V. and V. Ramanathan , 1989: Solar absorption by cirrus clouds and the tropical upper troposphere thermal structure. J. *Atmos. Sci*., **40**, 605 - 630

Sassen, K, and Z. Wang , 2002: Cirrus cloud icw water content radar algorithm evaluation using an explicit cloud microphysics model. *J. appl. Meteoro*l., **41**, 620-628.

Sassen, K, and L. Liao, 1996: Estimation of cloud content by W-band radar. *J. Appl. Meteor*., **35**, 932–938.

Sassen, K., 1987: Ice cloud content from radar reflectivity. J. Climate Appl. Meteor., **26**, 1050–1053.

Schneider, T. L., and G. L. Stephens, 1995: Theoretical aspects of modeling backscattering by cirrus particles at millimeter wavelengths. *J. Atmos. Sci*., **52**, 4367–4385.

Sekhon, S. R. and R.C. Srivastava ,1970: Snow size spectra and radar reflectivity. J. Atmos. Sci. **27**, 299-307.

Smith, P. L., 1984: Equivalent radar reflectivity factors for snow and ice particles. *J. Climate Appl. Meteor*., **27**, 1258-1260.

Sheppard, 1990: Measurement of raindrop size distributions using small Doppler radar. J. *Atmos. Oceanic Technol.,* **7**, 255–268.

Stephens, G. L., D. G. Vane, R. J. Boain, G. G. Mace, K. Sassen, Z.Wang, A. J. Illingworth, E. J. O'Connor, W. B. Rossow, S. L. Durden,S. D. Miller, R. T. Austin, A. Benedetti, C. Mitrescu and the CloudSat Science Team, 2002: The CloudSat Mission and the A Train. *Bull. Am. Meteorol. Soc., **83*****,*** 1771–1790.

Ryan, B. E., 2000: A bulk parameterization of the ice particle size parameterization and the optical properties in ice clouds. *J. Atmos. Sci.*, ***57***, 1436-1451.

Super, A.B., and E.W. Holyroyd, 1997: Snow accumulation algorithm development for the WSR_88D Radar. 28th Conf. on Radar Meteor., Austin, Texas, Amer. Meteor. Soc., U.S.A., 324-325.

Zawadzki, I, L. Ostiguy, and J.P.R. Laprise, 1993: Retrieval of the microphysical properties in a CASP storm by integration of a numerical kinematic model. *Atmosphere Ocean*, ***31***, 202 233.